Analyst

Analyst

PAPER

Characterization of core-shell MOF particles by depth profiling experiments using on-line single particle mass spectrometry

J. F. Cahill,[a] H. Fei,[b] S. M. Cohen[b] and K. A. Prather[b,c]

Materials with core-shell structures have distinct properties that lend themselves to a variety of potential applications. Characterization of small particle core-shell materials presents a unique analytical challenge. Herein, single particles of solid-state materials with core-shell structures were measured using on-line aerosol time-of-flight mass spectrometry (ATOFMS). Laser 'depth profiling' experiments verified the core-shell nature of two known core-shell particle configurations (<2 µm diameter) that possessed inverted, complimentary core-shell compositions (ZrO_2@SiO_2 versus SiO_2@ZrO_2). The average peak area ratios of Si and Zr ions were calculated to definitively show their core-shell composition. These ratio curves acted as a calibrant for an uncharacterized sample – a metal-organic framework (MOF) material surround by silica (UiO-66(Zr)@SiO_2; UiO = University of Oslo). ATOFMS depth profiling was used to show that these particles did indeed exhibit a core-shell architecture. The results presented here show that ATOFMS can provide unique insights into core-shell solid-state materials with particle diameters between 0.2-3 µm.

Introduction

Aerosol time-of-flight mass spectrometry (ATOFMS) has been used to characterize the chemical composition of small (0.2-3 µm) atmospheric aerosols over the last decade.[1, 2] Recently, ATOFMS has been used to characterize other particles beyond only atmospheric aerosols.[3-5] Uniquely, this technique uses a combination of lasers to measure the size and chemical composition of individual particles. Because ablation is laser based, simply tuning the power of the ionizing laser can selectively segregate the surface molecules of the particle from the core, creating a 'depth profile' of the major chemical constituents.[6-9] Using this ability of ATOFMS, the core-shell nature of small particles can be determined, a feat very few techniques can accomplish.[10] Depth profiling experiments have been demonstrated on atmospheric aerosols and polystyrene nanoparticles using a technique similar to ATOFMS, but these methods have not been reported to distinguish core-shell composition on other types of particles.[7-9]

The development of unique solid-state, core-shell nanomaterials represents an active field of research due to their wide variety of potential applications such as gas absorption,[11] catalysis,[12, 13] chemical sensing,[14] and drug delivery.[15-17] Through control of the chemical composition and thickness of the core and shell components, the physical and chemical properties of the material can be tuned to the needs of a particular application.[18] Silica, for example, offers advantages as a shell component such as high chemical stability.[15] Metal-organic frameworks (MOFs), constructed by joining inorganic secondary building units with organic linkers, have incredibly high surface areas and porosity. MOFs can be chemically tuned with functional groups, by varying metal ion composition, particle morphology, and guest molecules within the MOF.[3, 5, 19-21] A variety of core-shell MOFs have been created,[11, 15, 22-26] with a smaller number using silica as the shell component.[15, 17, 27]

Herein, the core-shell nature of two different nanoparticle structures with opposing core-shell composition, (ZrO_2@SiO_2 versus SiO_2@ZrO_2) was investigated using ATOFMS laser depth profiling experiments. An unknown, but expected core-shell MOF, UiO-66(Zr)@SiO_2 (UiO = University of Oslo), was verified to in fact be core-shell in nature. These results highlight the potential for this technique to investigate the core-shell structure of other nanomaterials, and to be a viable alternative characterization approach for core-shell solid-state materials with specified particle sizes.

Experimental

ATOFMS
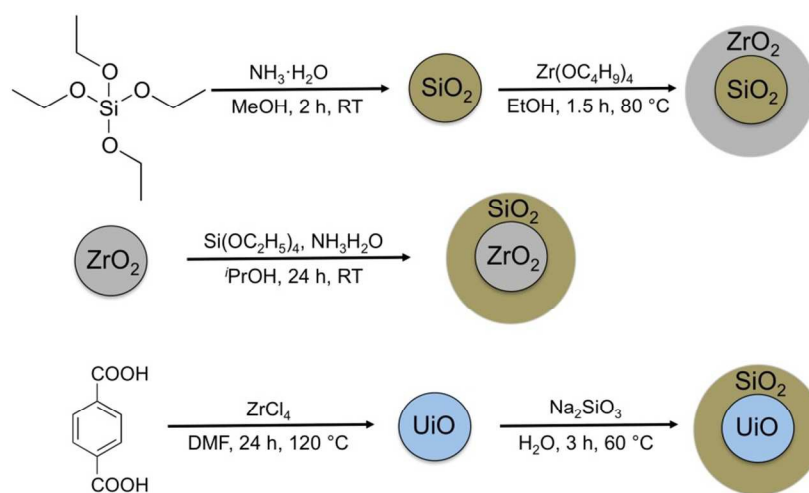
Fig. 1. Schematic for the synthesis of $SiO_2@ZrO_2$, $ZrO_2@SiO_2$, and UiO-66(Zr)@SiO_2.

A detailed discussion of the ATOFMS is available elsewhere.[28] Briefly the ATOFMS is capable of measuring both the size and chemical composition of single nanoparticles (0.2-3 μm in aerodynamic diameter). Mass spectra are generated using a 266 nm Nd:YAG laser to desorb and ionize the particle. At high laser powers (>1 mJ) the entire particle is desorbed; however, at lower laser powers (<1 mJ) it is unlikely that the whole particle is desorbed, but rather just molecules closer to the surface of the particle. Relative peak areas (RPA) (i.e. the fractional intensity of each peak in a mass spectrum) are used throughout this manuscript unless otherwise noted. ATOFMS spectra were processed in Matlab (Mathworks, inc.) using the YAADA toolkit (www.yaada.org).[29] In all figures error bars represent one standard deviation of the mean.

Preparation of nanomaterials

To standardize depth profiling experiments, known morphologies of solid-state materials were prepared. For this reason, Zr and Si were chosen, as core-shell nanomaterials $ZrO_2@SiO_2$ and $SiO_2@ZrO_2$ could be synthesized with sizes similar to common UiO-66 particles.

GENERAL METHODS: Starting materials and solvents were purchased and used without further purification from commercial supplies (Sigma-Aldrich, Alfa Aesar, EMD, TCI, and others).

SYNTHESIS OF $SiO_2@ZrO_2$: Synthesis of $SiO_2@ZrO_2$ core-shell particles was prepared as previously described.[30]

SYNTHESIS OF $ZrO_2@SiO_2$: Synthesis of $ZrO_2@SiO_2$ core-shell particles was prepared by a sol-gel method, with modification to a previous reported approach.[31] ZrO_2 core particles (ZrO_2, powder, 5 μm, 99% trace metals basis) were purchased from Sigma-Aldrich. SiO_2 coating of ZrO_2 was carried out by dispersing 45.9 mg ZrO_2 dispersion in 1 mL water. Then, 0.5 mL ammonia (28-30% aqueous solution) and 20 mL isopropanol were added to the ZrO_2 dispersion. After 30 min, 387 mg TEOS (tetraethoxysilane, $Si(OCH_2CH_3)_4$) was added with stirring. The mixture was stirred at room temperature for 24 h, and the product was separated via centrifugation at 6500 rpm for 15 min, washed with water (3×15 mL), and dried under vacuum at 70 °C.

SYNTHESIS OF UiO-66@SiO_2: The schematic for the synthesis of the core-shell solid-state materials is shown in Fig. 1.[15, 30, 31] Solvothermal synthesis of UiO-66 was carried out by dissolving $ZrCl_4$ (16 mg, 0.07 mmol), terephthalic acid (11.6 mg, 0.07 mmol), and acetic acid (210 mg, 3.5 mmol) in 4 mL DMF in a scintillation vial. The vial was then transferred to an isothermal oven at 120 °C for 24 h. After cooling, the solids were separated by centrifugation, and soaked in MeOH for 3 d before vacuum drying. Silica coating of MOF particles was performed by using a modified version of a reported procedure.[15] 10 mg of UiO-66 nanoparticles were dispersed in 4 mL of water. Sodium silicate ($Na_2SiO_3·5H_2O$, 47.5 mg, 0.224 mmol) was dissolved into 2 mL water, and the pH of the silicate solution was adjusted to ~7 using HCl. The silicate solution was added to the UiO-66 suspension, and the reaction was diluted to a volume of 20 mL with water. The suspension was stirred for 3 h at 60 °C. The particles were isolated by centrifugation, washed with water and ethanol, and dried under vacuum.

Results and discussion

Single Particle Depth Profiling

To effectively determine the core-shell composition of a material by ATOFMS, a number of key instrumental factors must be taken into account, namely: (1) ionization laser power,[32, 33] (2) peak ion sensitivities,[34, 35] and (3) changing matrix effects as a function of laser power.[35-37] Laser power is difficult to characterize as the effective laser power the particle experiences is dependent on the position of the particle within the Gaussian laser beam and laser shot-to-shot fluctuations. Both create variance in the effective depth sampled by ATOFMS. Peak ion sensitivities and matrix effects are more difficult to characterize as both effects could potentially vary with laser power. This is further complicated by the appearance or disappearance of ions at a specific mass/charge (*m/z*) of interest as a function of laser power. These problems can be circumvented by generating ion peak ratio curves using particles having known and complimentary core-shell architectures, which effectively serve as a standard to compare an unknown against. In this way, peak ratio trends of an unknown can be compared against known core-shell peak ratio curves and identified.[8]

For depth profiling experiments, laser power was varied from 0.1 mJ – 1.7 mJ ($4·10^6$ – $6·10^7$ W/cm^2). Laser power was measured to provide a general indication of the degree of laser variability, presented as the standard deviation in laser power. To mitigate the uncertainty caused by the position of the particle within the Gaussian beam profile, 500-1000 particles were collected at each laser power, with the exception of the lowest laser power for which ~100 particles were collected, due to being near the threshold of ionization at this laser power. It should be noted that Si and Zr ions are easily
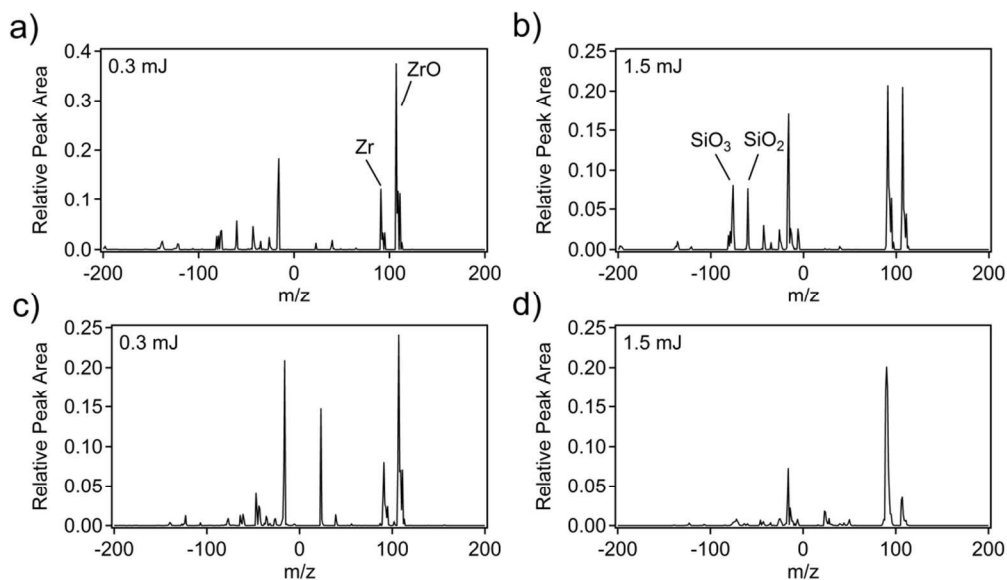
Fig. 2. Mass spectra of $SiO_2@ZrO_2$ (a-b) and $ZrO_2@SiO_2$ (c-d) at high and low laser power.

distinguishable in the particle mass spectra and that no other UiO-66 organic ions overlap with these peaks, which is a necessary requirement for successful depth profiling experiments.

Core-Shell $ZrO_2@SiO_2$ and $SiO_2@ZrO_2$ nanomaterials

Core-shell $ZrO_2@SiO_2$ and $SiO_2@ZrO_2$ particles were synthesized using previously described methods with slight modifications (see Experimental Section). The resulting particles were characterized by scanning and/or transmission electron microscopy (Fig. S1). Average mass spectra of $ZrO_2@SiO_2$ and $SiO_2@ZrO_2$ nanomaterials collected at high and low laser powers are shown in Fig. 2. Zr ions appear in the positive ion mode at m/z 89-95 (Zr^+) and 106-111(ZrO^{+-}).[4, 38] The mass spectra qualitatively show the expected core-shell nature of the materials. In the $SiO_2@ZrO_2$ particles, Si ions increase in intensity as the laser power is increased (Fig. 2(a, b)), indicating more Si present at the core of the particle. In contrast, Zr ions increase relative to Si ion between Fig. 2(c,d) representing more Zr content at the core of the particle, as expected for $ZrO_2@SiO_2$.

To compare total metal ion content, ion peak ratios, taken as the sum of average Si RPA for ions (m/z 60, 75-78) divided by the sum of average Zr RPA for peaks (m/z 89-95, 106-111), are shown in Fig. 3. Hereafter these m/z designations are referred to as the Si and Zr content, respectively. As expected the two materials have opposing slopes indicating differing core-shell composition. The minimum laser power to generate ions for both materials was 0.2-0.3 mJ. At 0.2 mJ, $ZrO_2@SiO_2$ begins at a mean peak ratio of 0.043 which steadily decreases to 0.020 by 1.7 mJ. $SiO_2@ZrO_2$ had a positive slope with a peak ratio starting at 0.153 at 0.3 mJ which increased with increasing laser power to 0.257 at 1.5 mJ. These two ratio curves inherently contain ATOFMS peak biases and hence provide a qualitative range of peak shapes for which an unknown core-shell material can be compared against.

It is important to note that the position of the lines in Fig. 3 (starting at highest laser power) represent the overall Si/Zr content difference between the materials. At the highest laser power, the particle is completely desorbed and thus the ratio obtained is indicative of all molecules in the particle. The core/shell nature of the material is identified by the trend of these points from their ratio measured at the highest laser power. To make this difference

clearer, the overall Si/Zr content collected for each set of particles obtained at the highest laser power (>1.5 mJ) was normalized to a value of 1. For reference, a trend with no slope indicates a homogeneous mixture of Si/Zr, while a ratio trend towards smaller or larger ratios indicates more Zr or Si at the surface of the particle, respectively. The normalized peak ratio trends for $ZrO_2@SiO_2$ and $SiO_2@ZrO_2$ are given in Fig. 4. The $SiO_2@ZrO_2$ ratio has a shallow slope towards smaller values, indicating a Zr shell. The increased ATOFMS sensitivity of Zr over Si likely biases this trend to have a
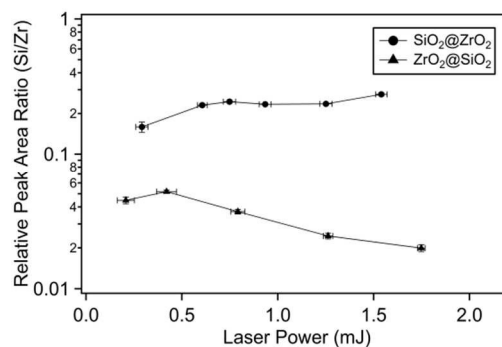
Fig. 3. RPA ratios Si/Zr of $SiO_2@ZrO_2$ (circles) and $ZrO_2@SiO_2$ (triangles).
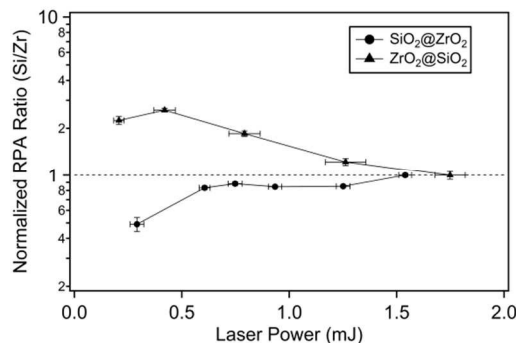
Fig. 4. Normalized RPA ratios (Si/Zr) of $SiO_2@ZrO_2$ (circles) and $ZrO_2@SiO_2$ (triangles).
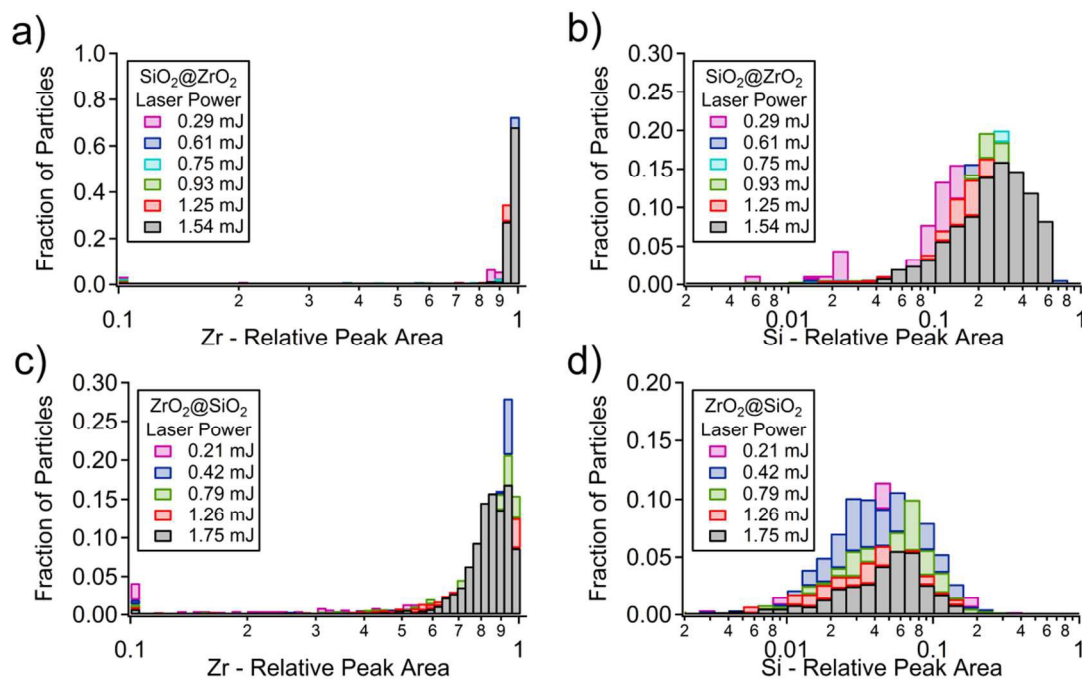
Fig. 5. Si and Zr single particle RPA distributions of $SiO_2@ZrO_2$ (a,b) and $ZrO_2@SiO_2$ (c,d).
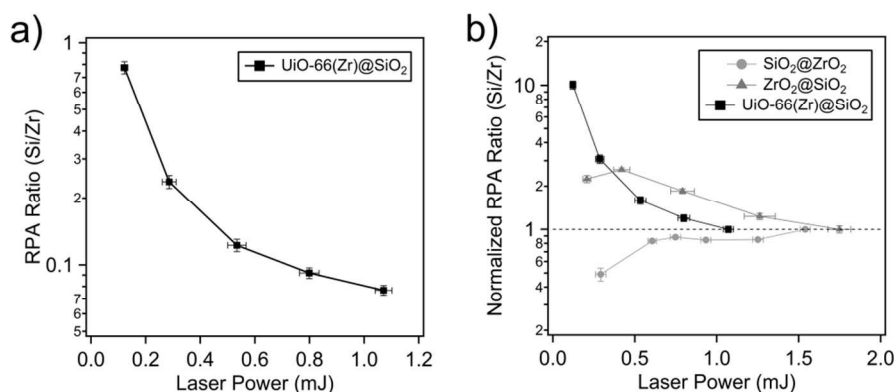
Fig. 6. Si/Zr RPA ratios: (a) and normalized ratios, (b) of UiO-66(Zr)@SiO$_2$. Normalized ratios of $SiO_2@ZrO_2$ and $ZrO_2@SiO_2$ are shown for reference.

relatively small slope. In contrast, the $ZrO_2@SiO_2$ trend sharply deviates towards higher ratios indicating more Si content at lower laser powers and thus more Si content at the surface.

These trends can be understood in another way, by looking at single particle RPA distributions. Single RPA distributions for Zr and Si from $ZrO_2@SiO_2$ and $SiO_2@ZrO_2$ are given in Fig. 5(A, B) and (C, D), respectively. These figures reflect all individually measured single particle RPAs used to calculate the mean ratios shown in Fig. 3. It can be seen in these figures that the trend of the peak ratio curve is predominantly governed by the core component. For $SiO_2@ZrO_2$ the mode of the Zr ion distribution stays relatively constant at a RPA of 0.9 for all laser powers. Additionally the number fraction of particles containing Zr is high (>0.95) and essentially constant across laser power. Assuming that the entire shell is desorbed at all laser powers, true for a relatively thin shell material, the relative ion content of Zr in the positive ion spectra would not change as laser power is increased further. In contrast, as laser power is increased the relative contribution of the core material increases, which is reflected as an increase in the mode of the Si peak distribution towards larger RPA, from 0.13 to 0.25. The same reasoning can explain $ZrO_2@SiO_2$, where the shell content (Si)

remains relatively constant (0.04-0.05) with laser power while the core content (Zr) increases with increasing laser power, in this case reflected by an increase in the number fraction of particles containing >70% Zr RPA, from 74-85% for 0.2 and 1.7 mJ, respectively.

Investigation of an unknown core-shell UiO-66(Zr)-SiO$_2$

With trends measured for nanomaterials of two opposing core-shell compositions, the Zr/Si content of an uncharacterized sample could be investigated. A MOF material encased in silica, hypothesized to be a UiO-66(Zr)@SiO$_2$ core-shell material, was synthesized. Single particle peak ratios collected for this material are shown in Fig. 6(a). The slope of the line is clearly negative and qualitatively similar in shape to $ZrO_2@SiO_2$ indicating that the UiO-66 contains a Si shell. At 1.1 mJ, the average peak ratio was 0.069, but as laser power decreased the peak ratio quickly increased to 0.711. The UiO-66(Zr)@SiO$_2$ ratio trend normalized in the same manner as described previously is shown in Fig. 6(B). For visual reference the $ZrO_2@SiO_2$ and $SiO_2@ZrO_2$ normalized trends are also included. Here it becomes immediately apparent that the UiO-66

peak ratio trend matches much more closely to that obtained with the $ZrO_2@SiO_2$ standard. Note that the range of laser powers used for UiO-66 were lower as the ionization threshold of the MOF was lower by ~0.1 mJ than in $ZrO_2@SiO_2$ and $SiO_2@ZrO_2$. This is likely due to increased laser absorption of organic molecules present in the MOF. If this difference were to be normalized the UiO-66(Zr)@SiO_2 and $ZrO_2@SiO_2$ ratio trends become even more similar. The ratio trend of UiO-66 increases more sharply than $ZrO_2@SiO_2$ perhaps indicating a more distinct core-shell, though with the current data this cannot be conclusively determined. Single particle RPA distributions were similar to those described for $ZrO_2@SiO_2$.

Conclusions

Particles of a core-shell MOF, UiO-66(Zr)@SiO_2, were Definitive characterization was determined using peak ratio curves of materials with similar chemical compositions to UiO-66(Zr)@SiO_2 but having known and opposing core-shell composition. It should be noted that all the data presented herein were collected from individual nanoparticles, 0.1-3 μm in aerodynamic diameter, rather than from large (>100 μm) crystals typically used to determine the core-shell nature of MOF materials.[11, 22-26]

The current limitation of this technique is the need to know instrument sensitivity as a function of laser power for a particular matrix composition; i.e. knowledge *a priori* of slopes of opposing core-shell compositions when measured by ATOFMS. The MOFs in this study were selected based on the availability of core-shell nanomaterials comprised of the same predominant ions present in the unknown MOF (Zr and Si) in order to provide context to the ATOFMS depth profile. As demonstrated herein, this limitation can be overcome if materials with known and opposing core-shell compositions are available. This technique also has the potential for quantitative measurement of shell thickness, provided that a more thorough accounting of the materials properties, ion formation mechanisms, and matrix effects is conducted.[8, 9] Future work will investigate the core-shell nature of other materials including a wider array of core-shell MOFs.

Acknowledgements

Notes

[a] Organic and Biological Mass Spectrometry Group, Chemical Sciences Division, Oak Ridge National Laboratory, Oak Ridge, Tennessee 37831-6131

[b] Department of Chemistry and Biochemistry, University of California, La Jolla, California, 920372

[c] Scripps Institution of Oceanography, University of California, La Jolla, California

Electronic Supplementary Information (ESI) available: Transmission electron microscopy images of $ZrO_2@SiO_2$ and $SiO_2@ZrO_2$ See DOI: 10.1039/b000000x/

References

1. K. A. Prather, T. Nordmeyer and K. Salt, *Analytical Chemistry*, 1994, **66**, 1403-1407.
2. T. Nordmeyer and K. A. Prather, *Analytical Chemistry*, 1994, **66**, 3540-3542.
3. M. Kim, J. F. Cahill, H. H. Fei, K. A. Prather and S. M. Cohen, *Journal of the American Chemical Society*, 2012, **134**, 18082-18088.
4. M. Kim, J. F. Cahill, K. A. Prather and S. M. Cohen, *Chemical Communications*, 2011, **47**, 7629-7631.
5. M. Kim, J. F. Cahill, Y. X. Su, K. A. Prather and S. M. Cohen, *Chemical Science*, 2012, **3**, 126-130.
6. E. Woods, G. D. Smith, R. E. Miller and T. Baer, *Analytical Chemistry*, 2002, **74**, 1642-1649.
7. A. Pegus, D. Kirkwood, D. B. Cairns, S. P. Armes and A. J. Stace, *Physical Chemistry Chemical Physics*, 2005, **7**, 2519-2525.
8. T. D. Vaden, C. Song, R. A. Zaveri, D. Imre and A. Zelenyuk, *Proceedings of the National Academy of Sciences of the United States of America*, 2010, **107**, 6658-6663.
9. A. Zelenyuk, J. Yang, C. Song, R. A. Zaveri and D. Imre, *Journal of Physical Chemistry A*, 2008, **112**, 669-677.
10. A. M. Katzenmeyer, J. Canivet, G. Holland, D. Farrusseng and A. Centrone, *Angewandte Chemie International Edition*, 2014, **53**, 2852-2856.
11. K. Hirai, S. Furukawa, M. Kondo, H. Uehara, O. Sakata and S. Kitagawa, *Angewandte Chemie-International Edition*, 2011, **50**, 8057-8061.
12. G. A. Somorjai and R. M. Rioux, *Catalysis Today*, 2005, **100**, 201-215.
13. Y. Li, G. Lu and J. Ma, *RSC Advances*, 2014, **4**, 17420-17428.
14. L. C. He, Y. Liu, J. Z. Liu, Y. S. Xiong, J. Z. Zheng, Y. L. Liu and Z. Y. Tang, *Angewandte Chemie-International Edition*, 2013, **52**, 3741-3745.
15. K. M. L. Taylor-Pashow, J. Della Rocca, Z. G. Xie, S. Tran and W. B. Lin, *Journal of the American Chemical Society*, 2009, **131**, 14261-+.
16. K. Khaletskaya, J. Reboul, M. Meilikhov, M. Nakahama, S. Diring, M. Tsujimoto, S. Isoda, F. Kim, K. I. Kamei, R. A. Fischer, S. Kitagawa and S. Furukawa, *Journal of the American Chemical Society*, 2013, **135**, 10998-11005.
17. W. J. Rieter, K. M. Pott, K. M. L. Taylor and W. B. Lin, *Journal of the American Chemical Society*, 2008, **130**, 11584-+.
18. J. Wang and X. C. Zeng, in *Nanoscale Magnetic Materials and Applications*, eds. J. P. Liu, E. Fullerton, O. Gutfleisch and D. J. Sellmyer, Springer US, 2009, pp. 35-65.
19. Z. Q. Wang and S. M. Cohen, *Chemical Society Reviews*, 2009, **38**, 1315-1329.
20. S. M. Cohen, *Chemical Science*, 2010, **1**, 32-36.
21. H. X. Deng, C. J. Doonan, H. Furukawa, R. B. Ferreira, J. Towne, C. B. Knobler, B. Wang and O. M. Yaghi, *Science*, 2010, **327**, 846-850.
22. M. Kondo, S. Furukawa, K. Hirai and S. Kitagawa, *Angewandte Chemie-International Edition*, 2010, **49**, 5327-5330.

23. K. Koh, A. G. Wong-Foy and A. J. Matzger, *Chemical Communications*, 2009, 6162-6164.

24. X. Song, T. K. Kim, H. Kim, D. Kim, S. Jeong, H. R. Moon and M. S. Lah, *Chemistry of Materials*, 2012, **24**, 3065-3073.

25. Y. Yoo and H. K. Jeong, *Crystal Growth & Design*, 2010, **10**, 1283-1288.

26. S. Furukawa, K. Hirai, K. Nakagawa, Y. Takashima, R. Matsuda, T. Tsuruoka, M. Kondo, R. Haruki, D. Tanaka, H. Sakamoto, S. Shimomura, O. Sakata and S. Kitagawa, *Angewandte Chemie-International Edition*, 2009, **48**, 1766-1770.

27. W. J. Rieter, K. M. L. Taylor and W. B. Lin, *Journal of the American Chemical Society*, 2007, **129**, 9852-+.

28. E. Gard, J. E. Mayer, B. D. Morrical, T. Dienes, D. P. Fergenson and K. A. Prather, *Analytical Chemistry*, 1997, **69**, 4083-4091.

29. J. O. Allen, *Arizona State University*, 2002, http://www.yaada.org.

30. J. M. Kim, S. M. Chang, S. Kim, K. S. Kim, J. Kim and W. S. Kim, *Ceramics International*, 2009, **35**, 1243-1247.

31. X. L. Yang, N. Zhao, Q. Z. Zhou, C. Cai, X. L. Zhang and J. Xu, *Journal of Materials Chemistry C*, 2013, **1**, 3359-3366.

32. R. J. Wenzel and K. A. Prather, *Rapid Communications in Mass Spectrometry*, 2004, **18**, 1525-1533.

33. P. T. Steele, A. Srivastava, M. E. Pitesky, D. P. Fergenson, H. J. Tobias, E. E. Gard and M. Frank, *Analytical Chemistry*, 2005, **77**, 7448-7454.

34. D. S. Gross, M. E. Galli, P. J. Silva and K. A. Prather, *Anal Chem*, 2000, **72**, 416-422.

35. P. V. Bhave, J. O. Allen, B. D. Morrical, D. P. Fergenson, G. R. Cass and K. A. Prather, *Environmental Science & Technology*, 2002, **36**, 4868-4879.

36. K. P. Hinz and B. Spengler, *Journal of Mass Spectrometry*, 2007, **42**, 843-860.

37. X. Y. Qin, P. V. Bhave and K. A. Prather, *Analytical Chemistry*, 2006, **78**, 6169-6178.

38. P. J. Silva, R. A. Carlin and K. A. Prather, *Atmospheric Environment*, 2000, **34**, 1811-1820.

Analyst Accepted Manuscript